13th International Symposium on Turbulence and Shear Flow Phenomena (TSFP13)
Montreal, Canada, June 25-28, 2024

ARTIFICIAL INTELLIGENCE CONTROL OF AN AHMED VEHICLE MODEL USING DISTRIBUTED JETS

Fan Dewei
Center for Turbulence Control,
Harbin Institute of Technology, Shenzhen
fandewei2014@hotmail.com

Deng Guoming
Center for Turbulence Control,
Harbin Institute of Technology, Shenzhen
dengguoming@hit.edu.cn

Zhou Yu
Center for Turbulence Control,
Harbin Institute of Technology, Shenzhen
yuzhou@hit.edu.cn

ABSTRACT

This work aims to investigate the active drag reduction (DR) of an Ahmed body with a rear slant angle $\varphi = 35°$, corresponding to the low-drag regime, using machine learning or artificial intelligence (AI) control at a Reynolds number $Re = 1.7 \times 10^5$ based on the square root of the body cross-sectional area. The AI control system comprises of five independently operated microjet arrays placed along the edges of the rear window and the vertical base, twenty-six pressure taps on the rear end of the body, and a controller based on ant colony algorism (ACA) for the unsupervised learning of near-optimal control laws or strategies that lead to the minimum cost function J. The J is designed to include both DR and input control energy, with a view to achieving energy saving as well as substantial DR. Both steady and unsteady microjet blowings are investigated, corresponding to 5 and 15 independent control parameters, respectively. While the optimal steady blowing strategy results in a maximum DR of 18%, the unsteady reaches 21%, both much higher than previous reports in the literature. However, given the same DR, the energy expenditure of the latter can be much smaller. Extensive flow measurements performed with and without control point to distinct mechanisms underlying the different control strategies.

INTRODUCTION

The generic Ahmed body is widely used as a simplified vehicle model in DR researches (Zhou & Zhang 2021), whose wake can be classified into two distinct regimes depending on the slant angle φ of its rear window, i.e., high-drag regime with $12.5° < \varphi < 30°$ and low-drag regime with $\varphi > 30°$. Zhang *et al.* (2015) and Liu *et al.* (2021) carried out relatively thorough investigations on the flow structures around the high and low-drag Ahmed bodies, respectively. Numerous studies have been performed on DR for the high-drag regime, with a significant DR reaching up to 29% achieved by Zhang *et al.* (2018). Nevertheless, reports on the control of a low-drag Ahmed body are scarce notwithstanding the fact that this body may represent the commonly used cars such as sport utility vehicle and multi-purpose vehicle, whose rear slant angles are usually larger than 30° (Zhou & Zhang 2021). Moreover, the maximum DR achieved so far for the low-drag regime is only about 4%. Then, several questions naturally arise. Could we develop an artificial intelligence (AI) control system that optimize five independently microjet arrays to achieve higher DR? Is there any interesting flow physics behind possible effective control? Based on our latest improved understanding of the flow physics (Liu *et al.* 2021), this work sets out to address the issues raised above through a rather extensive experimental investigation on active DR of a low-drag Ahmed body with $\varphi = 35°$ using five independent steady and unsteady microjets arranged at every edge of the rear end.

EXPERIMENTS DETAILS

Experiments were conducted in a closed-circuit wind tunnel with a test section 1.0 m high, 0.8 m wide and 5.6 m long. A flat plate was horizontally placed and 0.1 m from the floor to control the boundary layer thickness (Fig. 1). A ½-scaled Ahmed model ($\varphi = 35°$) was tested. The Reynolds number Re investigated is 1.7×10^5 based on the square root of the body cross-sectional area. Drag forces, surface pressure, hot-wire and PIV measurements were conducted. Five different actuations based on independently operated microjet arrays, referred to as C_1, C_2, C_3, C_4 and C_5, were deployed. C_1, C_3 and C_5 are three arrays of microjets along the upper and lower edges of the slanted surface and the lower edge of the base, respectively. C_2 and C_4 each comprise two microjet arrays, arranged along the two side edges of the rear window and the base, respectively. The blowing ratio of C_i ($i = 1, 2, \ldots, 5$) is defined by $BR^{Ci} = V_{ci}/U_\infty$, where V_{Ci} is the exit velocity of a microjet and U_∞ is the free-stream velocity. C_1, C_2, C_3, C_4 and C_5 produces a maximum DR of 9%, 1%, 5%, 1% and 7%, respectively. The right-handed Cartesian coordinate system (x, y, z) is defined in figure 1. In this paper, superscript asterisk '*' denotes normalization by $\sqrt{A}$ (= 0.167 m).

AI CONTROL SYSTEM

In the present control system, there are five control parameters of steady blowing or 15 control parameters of unsteady blowing to be optimized. It would be a challenge for conventional optimization techniques once the number of control parameters exceeds three; for instance, the extremum seeking method based on extended Kalman filter could be applied to at most three control parameters (Fan *et al.* 2020). On

the other hand, the AI control may get around this difficulty and may find the global optimum solution even when the number of control parameters is rather large, as demonstrated by Zhou *et al*. (2020).

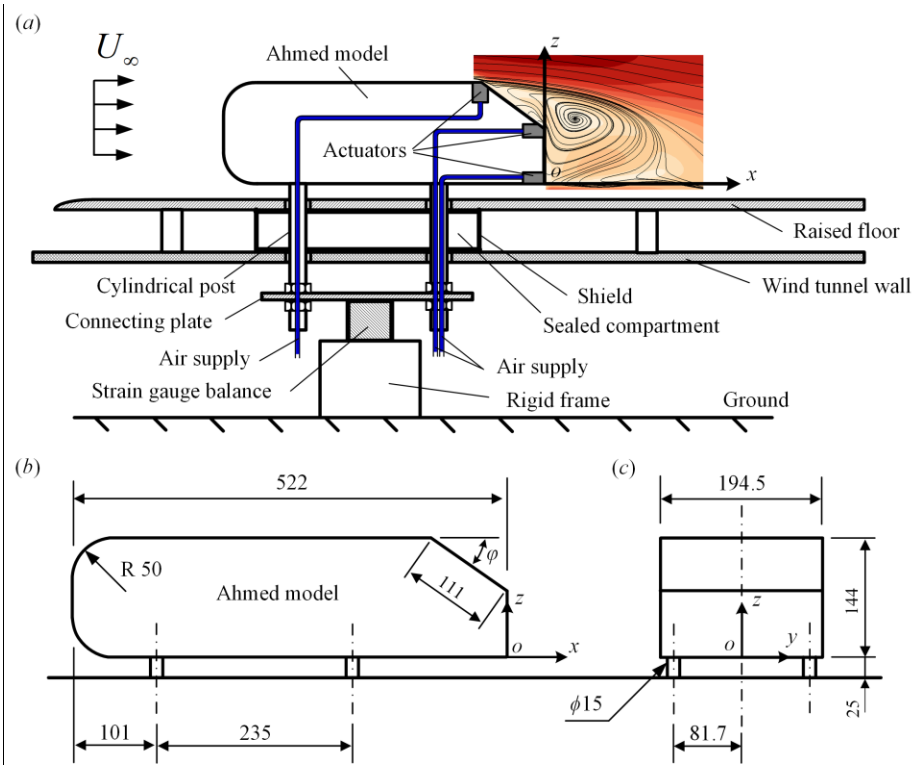

Figure 1. Schematic of experimental setup.

Ant colony algorism (ACA) is presently used. Inspired by the behavior of ant colonies in nature, Dorigo *et al*. (1991) proposed an approach for solving hard combinatorial or discrete problems. In their work, the well-known travelling salesman problem was used as an application example, and the ACA is manifested to be effective in finding out the optimal or shortest tour. The ACA uses many interacting agents, called artificial ants mimicking the real ones mediated by pheromone trails, and an algorithm based on positive feedback for exploring rapidly the optimal solution. Liao *et al*. (2014) developed a unified framework of ACA, in which the ants in each cycle are divided into two groups, one whose costs are below a threshold performing local search near the best ant, and the other executing global search in the entire parameter space. This method is demonstrated to be efficient in finding the global optimum solutions, when applied to more than 20 benchmark multimodal functions, without being trapped in local minima. They obtained the global extremum for every benchmark function with faster speed and higher accuracy, as compared with conventional ACA methods (Dorigo *et al*. 1991). This ACA was implemented presently for the first time as an algorithm of MLC in order to find the best control strategy for the DR of an Ahmed body wake, and is briefly introduced below.

The vector $\boldsymbol{B} = [b_1, b_2, \ldots, b_5]^{\mathrm{T}}$ or $[b_1, b_2, \ldots, b_{15}]^{\mathrm{T}}$ comprises all actuation commands or analog voltages, where the superscript 'T' denotes the transpose and b_i (i = 1, 2,…,5 or 15) regulates the mass flow controller for C_i (figure 2*a*). Then,

$$\boldsymbol{B} = \boldsymbol{K}(\boldsymbol{BR}, \boldsymbol{\alpha}, \boldsymbol{f_e}), \tag{1}$$

where $\boldsymbol{BR} = [BR^{C1}, BR^{C2}, \ldots, BR^{C5}]^{\mathrm{T}}$, $\boldsymbol{\alpha} = [\alpha^{C1}, \alpha^{C2}, \ldots, \alpha^{C5}]^{\mathrm{T}}$, $\boldsymbol{f_e} = [f_e^{C1}, f_e^{C2}, \ldots, f_e^{C5}]^{\mathrm{T}}$ are referred to as the control law of the combined actuations in this paper and $\boldsymbol{K}$ is the vector function that transforms $(\boldsymbol{BR}, \boldsymbol{\alpha}, \boldsymbol{f_e})$ to the control signals of the actuators. The optimization process searches for a law of form (1) that minimizes the cost

$$\boldsymbol{K_{opt}} = arg\ \min_{\boldsymbol{K}} J\left[\boldsymbol{K}(\boldsymbol{BR}, \boldsymbol{\alpha}, \boldsymbol{f_e})\right]. \tag{2}$$

The regression problem is to optimize mapping from five inputs of steady blowing or 15 inputs of unsteady blowing to a single output signal J and the optimizing process is schematically shown in figure 2(*b*), described briefly below:

Step 1: the process is initialized with a set of M = 100 randomly generated $\boldsymbol{B_m^n}$, m = 1, …, M, also called ants, for the first cycle of ACA (n = 1). Here, the superscripts 'n' and 'm' denote the cycle number and the mth control command of each cycle.

Step 2: each 'm' is experimentally tested for 25 s to yield the measured cost J_m^n. The pheromone (τ_m^n) is given by

$$\tau_m^n = (1 - e_v)\tau_m^{n-1} + J_m^n, \qquad (n = 1, \ldots, N), \tag{3}$$

where e_v is the evaporation rate and is set to 0.9, and N is the total number of cycles. The value of τ_m^0 is zero. Then, the ants are renumbered in order of the pheromone values, $\tau_1^n < \tau_2^n < \ldots < \tau_M^n$.

Step 3: the ants are sorted into two groups, one performing local search, and the other regenerated randomly in the entire search space. The transition probability (P_m^n) for the local search is written as

$$P_m^n = \begin{cases} 1, & p_m^n < p_0 \\ 0, & p_m^n \geq p_0 \end{cases}, \tag{4}$$

where p_0 is a threshold, which affects largely the ratio of ants that perform local or global searching. A right choice of p_0 may raise the efficiency of global searching of ACA, ensuring a relatively large number of ants to be generated randomly in the entire search space (or global searching). Otherwise, most ants may get engaged in local searching. The p_0 is presently chosen

to be 0.2 after a trial-and-error process. The p_m^n is a variation in τ_m^n relative to τ_1^n, viz.

$$p_m^n = \frac{\tau_m^n - \tau_1^n}{\tau_1^n}. \quad (5)$$

The ant conducting the local search is determined by

$$\boldsymbol{B}_m^{n+1} = \boldsymbol{B}_m^n + \frac{1}{2n}\boldsymbol{R}_a, \qquad \boldsymbol{R}_a = [r_1, r_2, \ldots, r_5]^{\mathrm{T}} \quad (6)$$

where r_i (i = 1, 2, …, 5) can be expressed by

$$r_i = 2S_i[\mathrm{rand}(0, 1) - 0.5], \quad (7)$$

and S_i denotes the maximum BR^{Ci}, α^{Ci} or f_e^{Ci} for C_i.

Step 4: next cycle starts with step 2 until the cost is converged to its minimum.

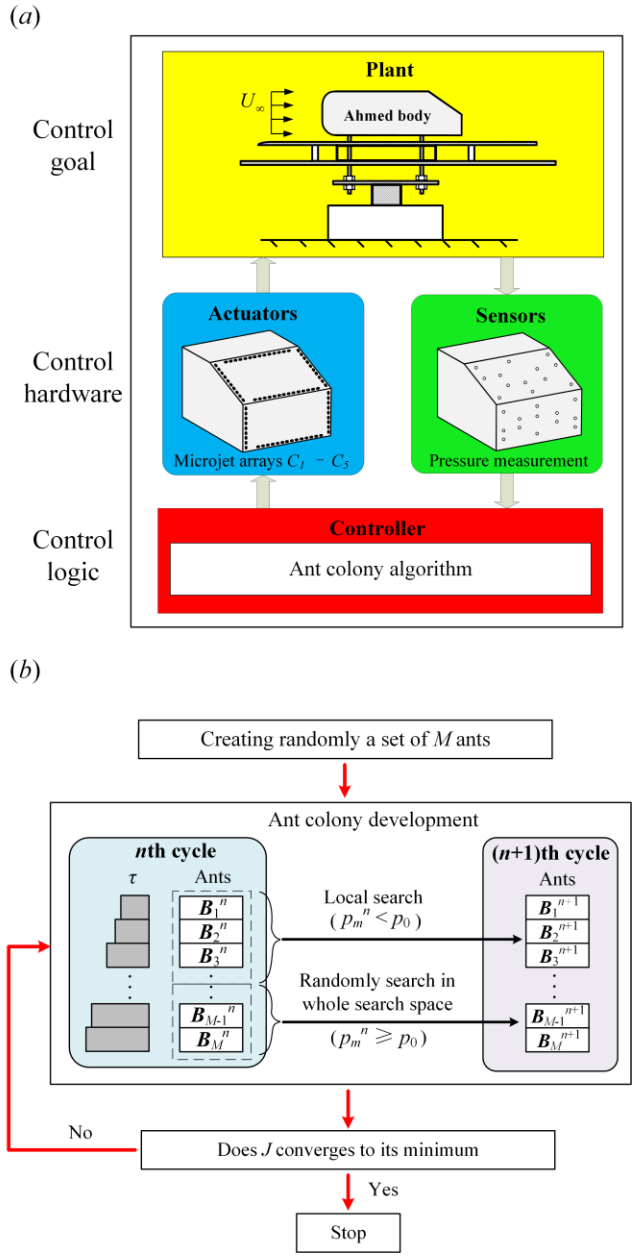

Figure 2. (*a*) Principle sketch of AI control system, which comprises the plant, sensors, actuators and an ant colony algorism (ACA) controller (*b*) Schematic of ant colony algorism.

The control law optimization process employed linear genetic programming is described briefly (figure 2*b*). Generally, AI acts as a regression solver to optimize a cost function associated with general nonlinear mappings, like the control law. The control system contains 4 steps: population creation (i.e., generate N_i=100 control laws), population evaluation (i.e., measure the performance of each control law), stop criterion check (i.e., check the best J) and population evolution (i.e., update generation based on the performance of last cycle).

RESULTS AND DISCUSSION

Combined actuations were deployed to seek the optimal modification of the interaction between different coherent structures in the wake. An AI control system was developed to search for the optimal control parameters for the maximum DR. This system comprises of the combined actuations, 26 pressure taps distributed on the rear end of the body, and a controller based on ant colony algorism (ACA) for the unsupervised learning of a near-optimal control law. The cost function J for the steady blowing is written as

$$J = -\langle \overline{C_p} \rangle + \alpha \sum_{i=1}^{5} (BR^{Ci})^3, \quad (8)$$

where C_p is the surface pressure coefficient; the overbar denotes time-averaging; the angular bracket expresses a quantity spatially averaged over the 26 pressure taps; α is a weighting factor.

The AI based on ACA algorithm is deployed to optimize the control parameters of all the five actuators. The cost of each ant was tested for 25 s in the optimization. The learning curve of the AI control for steady blowing was shown in figure 3(*a*). Each cycle consists 100 ants. The square symbol represents the best ant (A_n) in the nth cycle. The square symbol curve reveals the evolution of the best ant. After eight generations of optimization, the cost J of A_8 corresponding to $\boldsymbol{BR}$ = [5.8, 3.5, 4.9, 1.3, 1.8]$^{\mathrm{T}}$ drops substantially from J_0 = 0.235 to 0.166, and remains unchanged, implying a convergence of the cost that produces ΔJ of -29% associated with a DR of 18%. In contrast of the steady blowing, the learning curve of unsteady control was also shown in figure 3(*b*). The ant number of each cycle is 200. Up to the cycle n = 7, A_7 achieves the highest DR of 21% and the minimum cost J of 0.164. The optimal actuation frequency, duty cycle and blowing ratio of A_7 are $\boldsymbol{f}_e^*$ = [5.02, 3.08, 3.01, 3.95, 4.61]$^{\mathrm{T}}$, $\boldsymbol{\alpha}$ = [0.76, 0.46, 0.09, 0.76, 0.58]$^{\mathrm{T}}$ and $\boldsymbol{BR}$ = [2.15, 2.68, 0.45, 3.87, 3.59]$^{\mathrm{T}}$, respectively. The DR of unsteady blowing is larger than that of steady blowing. It is commenting that through the sensitivity analysis of DR to control parameters, under the condition of DR sacrifice of 3% for unsteady blowing, that is, yielding the same DR (18%) as the steady blowing, the efficiency may reach 30.6, which is much higher than that (0.13) of the steady blowing. The efficiency would be further increased to 52.1 when the DR of unsteady blowing decreases to 13%. This indicated the unsteady excitation is much more efficient than the steady blowing case.

One conceptual model of wake structures with the optimal control of steady blowing is proposed, as shown in figure 4. The altered wake is mainly characterized by a small separation bubble near the upper edge of the rear window, one pair of strong C-pillar vortices, and a patch of stagnated flow near the lower edge of the window due to the interaction between the attaching flow and the upstream and upward blowing of C_3, which results in a significant pressure rise near the mid lower end of the window. Moreover, the upper and lower recirculation bubbles take place behind the base. The shear layer separated from the side edges of the base is deflected inward due to the inward blowing of C_4, creating a boat tailing effect. The control efficiency η, which is defined by the ratio of the power saved

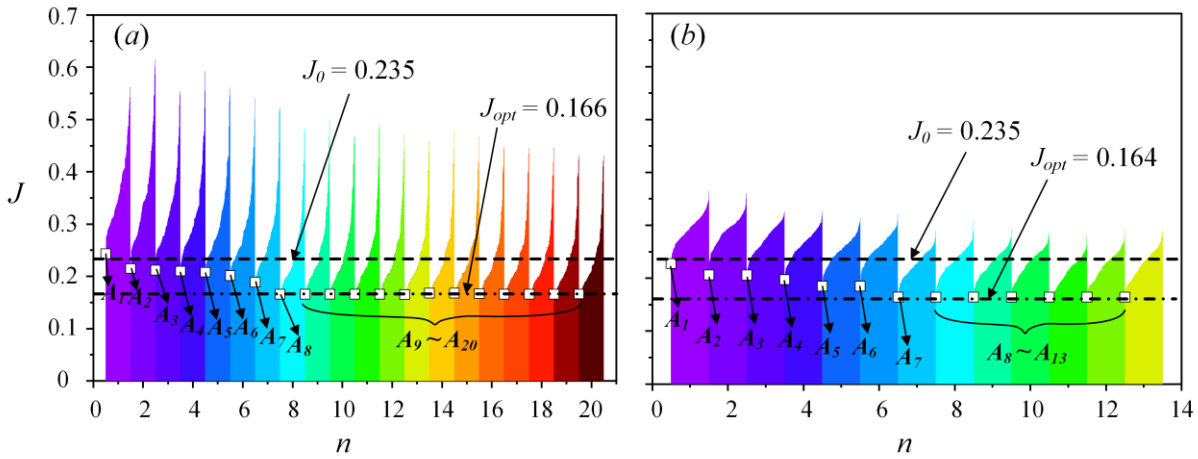

Figure 3. Learning curve of AI control based on ACA: (*a*) steady blowing, (*b*) unsteady.

from DR to the control input power, is evaluated. The optimal control is associated with a small η = 0.13. Nevertheless, it is found that a small sacrifice in DR may lead to a large increase in η; η rises with increasing sacrifice in *DR*, reaching 3.7 and 25.7 when DR drops to 16% and 10%, respectively. The flow modification of the most efficient control differs markedly from the optimal control. The pressure recovery on the rear part results largely from a downstream shift in two recirculation bubble centers.

Combined unsteady actuations, which were deployed separately at the same locations of C_1, C_2, C_3, C_4 and C_5, were also examined. The ACA-based AI control system was used to search for the optimal control parameters, including the frequency, duty cycle and blowing ratio of each actuation, for the maximum DR. The learning process converges after 7 cycles, with 1400 control laws tested. The optimal combination creates a maximum DR of 21%. A maximum η reaching up to 52.1, with a DR of 13%, was also obtained using the combined unsteady actuaitons. Further investigation is being conducted to gain a thorough understanding of flow physics and control mechanisms behind the optimal and the efficient control.

Work is under way to unveil the altered flow structures and control mechanisms under the combined unsteady actuations for the optimal and most efficient controls and will be presented during TSFP13.

CONCLUSIONS

Active DR of a low-drag Ahmed body has been extensively studied using five independently operated steady or unsteady

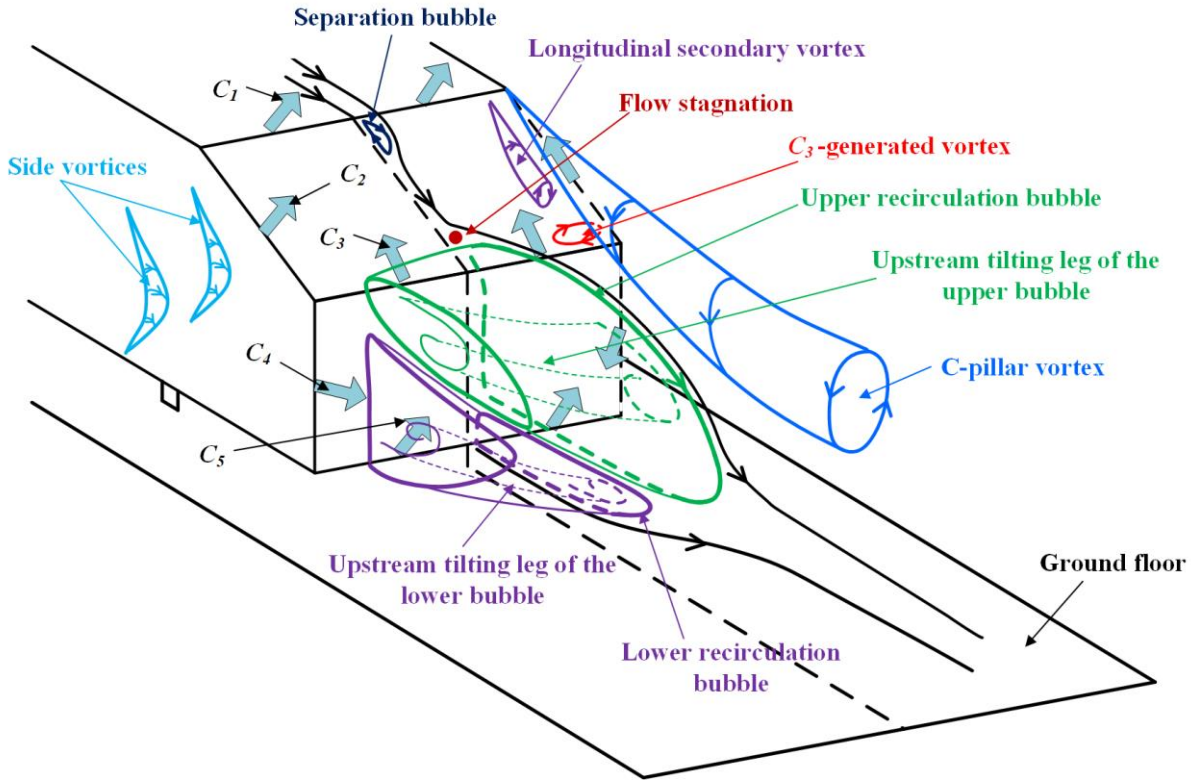

Figure 4. Conceptual model of flow structure under the optimized combination of C_1, C_2, C_3, C_4 and C_5.

blowing jet arrays. An AI control system was used to search for the best combination strategy for the five actuations. Major conclusions are as below:

(1) Under steady blowing, individual C_1, C_2, C_3, C_4 and C_5 produce DRs from 1% to 9%. The optimal combination of the five steady actuations or five independent control parameters found by the AI control creates a maximum DR reaching 18%, greatly higher than any previous report for a low-drag Ahmed body. The control efficiency can be greatly improved with a small sacrifice in DR. The η corresponding to the DR of 18% is only 0.13 but may rise to 3.7 and 25.7 given a sacrifice of DR by 2% and 8%, respectively. Modification in the flow structure under the optimal control or maximum DR is distinct from that under the most efficient control with η = 25.7. Under the optimal control, the two C-pillar vortices are greatly strengthened, inducing a downwash flow between them and flow reattachment over the rear window. The reattached flow interacts with the upward blowing of C_3, generating a stagnated flow near the lower end of the window and hence a big pressure increase, up to 287%, in this region, which is the main reason for the significant DR. On the other hand, the mechanism of the most efficient control is largely due to the longitudinal elongation of the upper and lower recirculation bubbles and the downstream shift of their centers. There is little change with the two C-pillar vortices.

(2) Under unsteady blowing, C_1, C_2, C_3, C_4 and C_5 produce DRs from 2% to 4%. Yet, with a significantly larger searching space (15 independent control parameters) than steady blowing, the optimal control performance is significantly improved, the maximum DR reaching 21%. Given the same DR (18%) as steady blowing, the control efficiency is 31, much higher than that (0.13) of steady blowing. Furthermore, the maximum efficiency may reach 52.1 with a corresonding DR of 13%. The flow structure modification under the optimized combination of the five unsteady actuations is distinct from its steady control couterpart. For instance, the strengthes of the two C-pillar vortices are reduced; flow separation from the upper edge of the rear window is suppressed, with one separation bubble occurring in the upper region of the window, whose size contracts substantially as compared with the unforced flow. This separation bubble interacts with the upstream recirculating flow from the base, producing a pressure recovery on the lower part of the window.

ACKNOWLEDGEMENTS

Authors wish to acknowledge support given to them from NSFC through grants 91952204 and 12202124, from the Research Grants Council of the Shenzhen Government through grant JCYJ20210324132816040 and from CGN-HIT Advanced Nuclear and New Energy Research Institute through Grant No. CGN-HIT202221.

REFERENCES

Dorigo, M., Maniezzo, V. & Colorni, A. 1991 Positive feedback as a search strategy. *Technical Report* 91-016.

Fan, D. W., Zhou, Y., & Noack, B. R. 2020. Fast triple-parameter extremum seeking exemplified for jet control. *Exp. Fluids* 61, 152.

Liao, T., Montes de Oca, M., Stützle, T. & Dorigo, M. 2014 A unified ant colony optimization algorithm for continuous optimization. *Eur. J. Oper. Res.* **234**, 597–609.

Liu, K., Zhang, B.F., Zhang, Y.C., Zhou, Y. Flow structure around a low-drag Ahmed body. Journal of Fluid Mechanics, 2021, 913, A21.

Zhang B.F., Zhou Y., To S. Unsteady flow structures around a high-drag Ahmed body. Journal of Fluid Mechanics, 2015, 777, 291-326.

Zhang, B.F., Liu, K., Zhou, Y., To, S., Tu, J.Y: Active drag reduction of a high-drag Ahmed body based on steady blowing. Journal of Fluid Mechanic, 2018, 856, 351-396.

Zhang B.F., Fan D.W., Zhou Y. Artificial intelligence control of a low-drag Ahmed body using distributed jet arrays. Journal of Fluid Mechanics, 2023, 963, A3.

Zhou, Y. & Zhang, B.F. Recent advances in wake dynamics and active drag reduction of simple automotive bodies. Applied Mechanics Reviews, 2021, 73, 060801